ADVANCED MATERIALS
www.advmat.de

Replicating the *Cynandra opis* Butterfly's Structural Color for Bioinspired Bigrating Color Filters

Xiaobao Cao, Ying Du, Yujia Guo, Guohang Hu, Ming Zhang, Lu Wang, Jiangtao Zhou, Quan Gao, Peter Fischer, Jing Wang, Stavros Stavrakis,* and Andrew deMello**

Multilayer grating structures, such as those found on the wings of the butterfly *Cynandra opis*, are able to interact with light to generate structural coloration. When illuminated and viewed at defined angles, such structural color is characterized by exceptional purity and brightness. To provide further insight into the mechanism of structural coloration, two-photon laser lithography is used to fabricate bioinspired bigrating nanostructures, whose optical properties may be controlled by variation of the height and period of the grating features. Through the use of both spectral measurements and finite-element method simulations, herein specific feature dimensions are identified that due to the combined effects of multilayer interference and diffraction generate excellent spectral characteristics and high color purity over the entire visible range. Additionally, it is demonstrated that variation of feature period and/or height plays a central role in controlling both hue and purity. Importantly, such tuneable bigrating structures are of significant utility in color filtering applications.

1. Introduction

Since Perkin's discovery of mauveine in 1856, synthetic dyes have found widespread use and application in almost all walks of modern life.[1] Despite their utility, synthetic dyes are environmentally damaging and limited in their brightness, purity (full width at half maximum, FWHM), and lifetime.[2] To overcome such limitations, much recent activity has focused on the generation of long-lasting colors via structural coloration, where color results from the interaction of visible light with periodic micro- or nano-structures causing diffraction, interference, and scattering.[3] Structural color produced in such a manner is usually angle-dependent (iridescent) and when compared to color produced by light absorption is more vibrant, tuneable, and stable.[4] To date, a variety of photonic structures have been used to generate structural color and replace traditional pigmentation. These include tuneable high-index photonic glasses, micron-sized spherical colloidal assemblies, and diffraction grating structures.[5,6] Although bio-inspired photonic structures have been used to create highly saturated structural color, they are difficult and costly to make and poorly suited to large-scale production. Moreover, there is as yet an unmet demand for new bio-inspired structural colors across the entire visible spectrum. Accordingly, a better understanding of the underlying mechanisms of structural coloration will undoubtedly lead to improved color properties and lifetimes.

Although numerous examples of structural color exist in nature, much interest has focused on the study of the photonic nanostructures of butterfly wings, due to their bright and iridescent color.[7,8] For example, Vigneron et al. showed that the rainbow iridescence effect produced by the wing scales of the *Pierella luna* (Moon Satyr) butterfly results from a macroscopic deformation of the entire scale, with illumination of the wing decomposing white light as a diffraction grating would

X. Cao, Y. Du, Q. Gao, S. Stavrakis, A. deMello
Institute for Chemical and Bioengineering
ETH Zürich
Vladimir Prelog Weg 1, Zürich 8093, Switzerland
E-mail: cao_xiaobao@gzlab.ac.cn; stavros.stavrakis@chem.ethz.ch; andrew@ethz.ch

X. Cao
Guangzhou Lab
International Bio Island
Haizhu District, Guangzhou, Guangdong, China

The ORCID identification number(s) for the author(s) of this article can be found under https://doi.org/10.1002/adma.202109161.

DOI: 10.1002/adma.202109161

Y. Du, Y. Guo, M. Zhang, L. Wang
College of Science
Zhejiang University of Technology
Liuhe Rd 288 Xihu, Hangzhou, Zhejiang 310014, China

G. Hu
Key Laboratory of Materials for High Power Laser
Shanghai Institute of Optics and Fine Mechanics
Chinese Academy of Sciences
Shanghai 201800, China

J. Zhou, P. Fischer
Institute of Food, Nutrition and Health
ETH Zürich
Schmelzbergstrasse 7, Zürich 8092, Switzerland

J. Wang
Institute of Environmental Engineering
ETH Zürich
Laura-Hezner-Weg 7, Zürich 8093, Switzerland

do, but in a reverse color sequence.[9] Alternatively, in the case of *Morpho* butterfly wings, a vivid structural blue color has been shown to arise as a consequence of multiple physical phenomena, including multilayer interference, diffraction, scattering, and pigment-based absorption.[10] Additionally, a combined experimental and theoretical study revealed that single *Lamprolenis nitida* butterfly wing scales comprise two separate blazed gratings that generate two iridescent colors.[11] Such "natural" optical structures have inspired scientists to use either template-based or biomimetic fabrication processes to generate structural color in artificially devised structures,[7,12,13] finding utility for example in photonic structures, thermal imaging sensors, infrared spectroscopy, and biosensors.[5,14]

Extensive studies of nano/microstructure arrays located in the wing scales of *Morpho* butterflies[15] have concluded that a network of longitudinal ridges acts as a diffraction grating to generate the vibrant blue coloration.[16] The interaction of light with 3D microstructures in such wing scales results in interference, reflection, and diffraction, producing colors that vary as a function of observation angle.[17] That said, surprisingly, few studies have focused on the design and fabrication of bio-inspired gratings that mimic the coloration produced by such nano/microstructures in butterfly wings. Recently, England et al., inspired by the reflective structures found in *P. luna* butterfly wings, fabricated a new type of quasi-planar grating and demonstrated that this can mimic the unusual diffraction properties of the biological structure (with a reversed color-order sequence) and be tailored to generate user-defined optical properties.[18] The most well-known organisms producing structural coloration are perhaps *Morpho* butterflies that produce a bright blue reflection color which remains stable across a wide range of viewing angles. This intense blue coloration has been comprehensively studied since it is far less angle-dependent than conventional optical diffraction gratings.[19] Multi-layered ridges found in the wing scales of *Morpho* butterflies generate a broad blue color, with the existence of positional disorder being essential for the angle-insensitivity of the produced color.[17] Inspired by these butterflies, Cary et al. reported the fabrication and optical characterization of periodic and quasi-periodic (with some positional disorder) multilayer polymeric nanostructures.[19] It is worth noting that in this case only the structural disorder configuration of the multilayer structure improves the broad-angle reflection of such diffraction gratings, and is fundamental for reducing the angular dependence of color. However, despite the outstanding optical properties of the aforementioned multilayer structures over wide observation angles, their weak transmittance below 500 nm[20] prohibits their use as broadband color filters. Thus, it still remains a challenge to produce a multilayer structure that provides for both high transmittance across the whole visible spectrum and color purity. In this regard, a particularly interesting optical structure termed a "crossed double-grating" was discovered several years ago in the wings of the *Cynandra opis* butterfly. Such a structure produces a blue iridescence when viewed with a light source over a narrow range of incident angles.[21] Importantly, such a crossed double-grating is not as complex to fabricate as the quasi-planar or quasi-periodic gratings found in the *P. luna* and Morpho butterfly wings, respectively. For example, the wings of the *Morpho* butterfly consist of tilted scales, with every scale comprising parallel rows decorated with complex nanostructures of ridges and lamellae.[12] The arrays of ridges and lamellae constitute the photonic crystal-like structures and cause multilayer interference producing the intense blue reflection.

Although progress has been made in understanding the origins of structural coloration in butterfly wings, a detailed analysis of the structure-property relationships associated with multilayer (bigrating) structures is needed, with a view to creating bespoke artificial materials for technological applications. Until recently, this has been a far from simple task due to the difficulties associated with fabricating appropriate and scalable micro- and nano-structures.[22] Fortunately, contemporary developments in additive manufacturing using two-photon polymerization (2PP) have established robust and precise routes for the fabrication of micro- and nano-structured devices on flexible substrates.[23] Leveraging such advances, we herein use two-photon photolithography to fabricate novel crossed bigrating structures, with negligible surface roughness and low optical loss in the visible region of the electromagnetic spectrum. 2PP is especially useful in this regard since it has been used to good effect in creating polymeric structures with a resolution down to 150 nm.[23] We show that incorporation of two crossed gratings within a single structure, mimicking features found in *C. opis* wings, allows the generation and tuning of structural color in a direct manner. Additionally, our integrative approach, combining optical microscopy/spectroscopy and finite-element method (FEM) simulations, enables the detailed investigation of the coloration mechanism within a variety of bigrating configurations.

2. Theory and Modeling

As noted, the "crossed double-grating" structures present in the wings of *C. opis* generate blue iridescence. Here, micron-sized ridges form a periodic array (termed plane 1), with the ribs of the grating forming a second underlying diffracting plane (termed plane 2) orthogonal to plane 1. Since both interference and diffraction effects contribute to coloration, we initially sought to decompose these two phenomena into two distinct processes. The first, applies the multi-film interference equation[24] to resolve interference between plane 1 and 2 (termed inter-planar interference as shown in Figure S1A, Supporting Information). The regular multi-layer structure acts as a Bragg mirror and in its infinite form is a 1-D photonic crystal.[25] Accordingly, the multi-film interference equation is given as,

$$m\lambda = 2(n_1 h_1 \cos\varphi_i + n_2 h_2 \cos\varphi_i) \quad (1)$$

where m is a positive integer, h_1 and h_2 are the heights of each grating in plane 1 and 2 respectively, n_1 and n_2 are the average refractive indices of the two gratings and φ_i is the angle of incidence. The second process resolves interference between different rows of "ribs" within the same plane (termed inter-rib interference in Figure S1B, Supporting Information) using the grating equation, that is,

$$d(\sin\varphi_i + \sin\varphi_d) = n\lambda \quad (2)$$

where n is a positive integer indicating the diffraction order, d is the grating period and φ_i *and* φ_d are the angles of incidence and diffraction, respectively. Inspection of Equation (2)

indicates that both the period and incident angle control spectral characteristics. When a beam of polychromatic light is incident on the bigrating, light is dispersed initially by plane 2 into multiple beams, with each of the transmitted beams being further diffracted by plane 1 (Figure S1B, Supporting Information). As shown in Table S1, Supporting Information, when the period of the upper grating in plane 1 is twice the period of the lower grating in plane 2, the diffraction wavelengths and angles associated with the +2-order peaks in plane 1 are the same as the +1-order peaks in plane 2. Moreover, when the resulting wavefronts from plane 2 pass through plane 1, the emerging wavefronts constructively interfere to produce a dense diffraction pattern with sharp and intense fringes. Accordingly, bigratings with well-defined periods can be used to direct light of certain wavelengths into specific directions. However, the anisotropy and 3D structure of the bigrating results in strong coupling between orthogonally polarized waves, and thus separate analysis of each grating will be insufficient when appreciable coupling occurs between diffracted orders.[26] To develop a better understanding of the generic structure, FEM simulations implemented in COMSOL Multiphysics 5.5 (COMSOL, Burlington, USA) were used to predict light intensity values from periodic microstructures. Equations (1) and (2), indicate that structural color will be controlled through variation of four parameters, namely d, h, n_{eff}, and φ_i. In this regard, our aim was to exploit the features of bigratings with two periods (d_1, d_2) and heights (h_1, h_2) to generate unique structural coloration over a wide wavelength range.

3. Results and Discussion

As previously noted, interference and diffraction can produce iridescent colors within structures possessing 3D periodicity.[27] Moreover, when diffraction is involved, coloration will be angle-dependent over a narrow angle range.[21] In the case of the male *C. opis* butterfly, a deep blue color is observed on specific regions of the wings (**Figure 1**A). As revealed by scanning electron microscopy (SEM) imaging of these regions (Figure 1B,C), the iridescent blue color is produced by a crossed double-grating like structure (i.e., a bigrating). Here, an array of ridges forms the first diffractive plane (plane 1), while the cross-ribs below this plane form the second diffracting plane (plane 2). Such a structure, formed by two orthogonal gratings, can diffract light in both the x and y directions.[28] Analysis of the SEM image in Figure 1C and atomic force microscopy (AFM) measurements indicate a period (d_1) of 1.18 µm and a height (h_1) of 2.1 µm for the upper grating. These values are approximately double those of the lower grating, where d_2 = 0.63 µm and h_2 = 0.98 µm. Such an array, consisting of both micro- and nano-structures, is a result of millions of years of evolution, with structural modifications being responsible for color variations between species.[29] We used a simplified bigrating structure (Figure 1D) to mimic the crossed double-grating structures found in *C. opis* wings. In all the tested configurations, the upper grating in plane 1 has a height h_1 and is periodic (with a period d_1) in the x-direction and uniform in the y-direction, whereas the lower grating in plane 2 has a height h_2 and is periodic (with a period d_2) in the y-direction and uniform in the x-direction. When white light is incident (across a wedge of angles) on the bigrating structure, highly saturated coloration is observed at certain output angles due to the combined effects of interference and diffraction (Figure 1E). Figure 1F shows a representative SEM image of a fabricated bigrating structure having d_1 = 800 nm and d_2 = 400 nm. The height profiles of the bigrating structure (h_1 = 200 nm, h_2 = 100 nm) are assessed by AFM imaging and presented in Figure S3, Supporting Information.

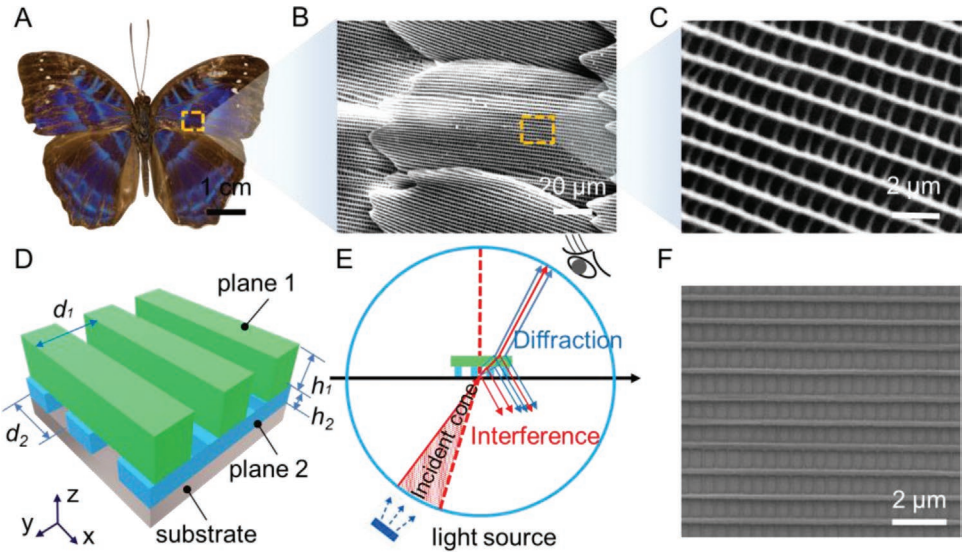

Figure 1. Microstructural components of the *C. opis* butterfly wing and its reconstruction. A) Photograph of a male *C. opis* butterfly exhibiting deep blue iridescence in specific regions of the wings. B) SEM micrograph of the iridescent blue scales of a *C. opis* wing. C) Selected enlargement of the scale region shown in panel b under high magnification, highlighting the existence of double-grating structures. D) Schematic illustration of the bigrating-based color filter model structure. Two grating layers are polymerized onto an ITO-coated glass substrate. E) Schematic illustration of structural coloration via interference and diffraction in the bigrating structure. F) SEM image of a 3D printed bigrating structure (d_1 = 800 nm and d_2 = 400 nm).

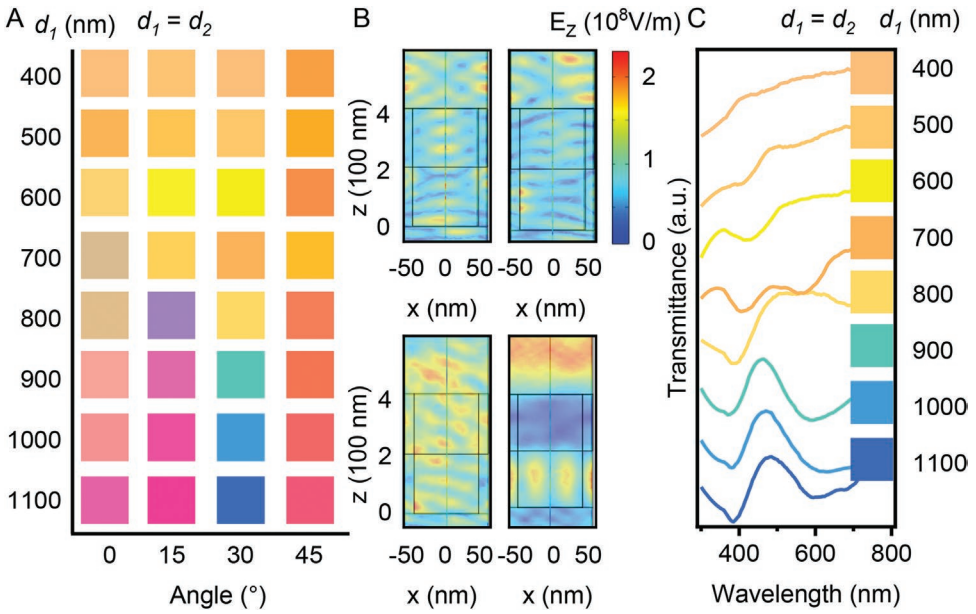

Figure 2. Influence of incident angle on structural coloration. A) Structural colors generated for different periods ($d_1 = d_2 = 400$–1100 nm) and varying incident angles (between 0° and 45°). B) Simulated electric field distribution (E_z) for the bigrating structure with $d_1 = d_2 = 900$ nm and incident angles of 0°, 15°, 30°, and 45°. C) Experimental transmission spectra between 300 and 800 nm.

3.1. Influence of Incident Angle, Period, and Height on Structural Coloration

We next examined how variations in both the incident angle and geometrical characteristics of the bigrating structures could be used to generate bespoke structural color. Specifically, we considered the case in which the orthogonal gratings share the same period and height, and thus can be treated as a single-layer grating. FEM simulations were performed to investigate the relationship between period structure and the resulting structural color spectra under different incident angles (**Figure 2**A). This was achieved by varying the grating period between 400 and 1100 nm (at 100 nm intervals), the incident angle from 0 to 45° and maintaining a grating height (h_1 and h_2) of 200 nm. It can be seen that when varying the incident angle between 0 and 45°, there was a negligible color change for grating periods between 400 and 500 nm. In contrast, for gratings with periods above 600 nm, color hue and purity are more sensitive to variations in incident angle. For example, for a grating period of 900 nm color is seen to change from light pink at 0°, to violet at 15°, cyan at 30°, and orange at 45°; with the latter exhibiting the highest purity (smallest FWHM).

Figure 2B presents transmitted electric field profiles in the *xz* plane for a wavelength of 500 nm, a grating period of 900 nm, a grating height of 200 nm, and incident angles of 0°, 15°, 30°, and 45°. The presented heat maps confirm that the transmitted intensity at 500 nm increases with increasing incident angle. However, scattering at angles greater than 30° increases rapidly, thereby decreasing total transmittance.[30] Adoption of an incidence angle of 30° provides the optimum balance between color purity and brightness, and thus all transmission spectra presented in Figure 2C are simulated for this incidence angle. Additionally, when the grating period is comparable in magnitude to visible light wavelengths (i.e., 300–800 nm), the structure can be approximated as a thin film, and thus diffraction will not contribute significantly to the optical characteristics. For larger periods (between 900 and 1100 nm), diffraction occurs at large incidence angles and structures exhibit a strong violet color.[2] In this regard, our results are in good agreement with the work of Brink and Lee, who noted that deviations in the grating period (d_1 and d_2) within *C. opis* wings are the primary factors controlling the spectral distribution of diffracted light.[21]

To more closely investigate the relationship between grating height and structural color, we numerically simulated transmission spectra for two bigrating structures having the same period (of 800 nm) but different grating heights (where h_1 is varied whilst keeping h_2 constant and vice versa; **Figure 3**A). As expected, these simulations indicate that color variations are height dependent, since the two periodic structures form a lattice of diffracting elements. More specifically, Figure 3B,C shows that increases in either h_1 or h_2 (at constant h_2 or h_1, respectively) cause the primary spectral peak to shift to longer wavelengths (as indicated by the dashed lines). This trend is observed regardless of the relative heights of h_1 and h_2, but it should be noted that color purity is enhanced when $h_1 > h_2$ (Figure 3B). In addition, since the total height of both bigrating structures shown in Figure 3A is the same (as well as their effective refractive index), one might expect (according to Equation (1)) that the resulting transmission spectra should be identical. However, the observed differences in the transmission spectra result as a consequence of the difference in h_1 and h_2, which contribute to different diffraction properties as defined by Equation (2). Indeed, it should be noted that although it is possible to achieve dynamic color filtering through adjustment of the periodicity alone (Figure 2), a more effective route to filtration is via the alteration of the bigrating height (Figure 3).

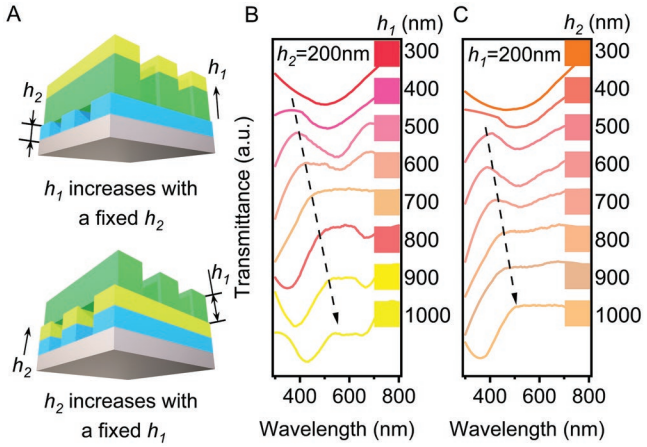

Figure 3. Comparison of influence of the height of plane 1 (h_1) and plane 2 (h_2). A) Schematics of two bigrating structures with a fixed period of 800 nm but different grating heights. B) Simulated transmission spectra and associated bigrating colors as a function of h_1 (between 300 and 1000 nm) and a constant h_2 of 200 nm. C) Simulated transmission spectra and associated bigrating colors as a function of h_2 (between 300 and 1000 nm) and a constant h_1 of 200 nm.

3.2. Influence of the Period Ratio (d_1:d_2) on Structural Coloration

To investigate the relationship between the period ratio (d_1:d_2) and structural color, we systematically varied the ratio d_1:d_2 between 1:1 and 3:1 (i.e., 300 nm/300 nm, 450 nm/300 nm, 600 nm/300 nm, 750 nm/300 nm to 900 nm/300 nm), whilst keeping the grating heights fixed (i.e., $h_1 = h_2 = 300$ nm). **Figure 4**A displays both experimental and simulated spectra (and associated bigrating colors images) for five different period ratios, where $h_1 = h_2 = d_2 = 300$ nm. As the period ratio varies, the bigrating structures exhibit different transmission spectra and render colors ranging from orange to deep blue. It can be also observed that achromatic colors can be produced using bigrating configurations with a period ratio between 1:1 and 1.5:1. This clearly demonstrates that tunability of the grating period allows the bigrating structures to produce either chromatic or achromatic colors. Similar achromatic colors are generated by the wing scales of the basal moth *Micropterix aureatella*.[31] It should be noted that the observed differences between corresponding simulated and experimental transmittance spectra are primarily a result of (nm-scale) drift during the two-photon lithography process. Nevertheless, the similarity of spectral profiles in the visible region and the color pallets for both experimental and simulated data confirm the utility of the developed model.

The FWHM of the primary spectral peak from each spectrum shown in Figure 4A decreases as d_1:d_2 increases from 1:1 to 3:1, indicating that the highest color purity is obtained at large d_1:d_2 ratios (Figure 4B). The peak intensity for each spectrum remains essentially constant when d_1:d_2 varies from 1:1 to 2:1, but decreases when d_1:d_2 ratios exceed 2:1, due to increased scattering occurring in high aspect ratios bigratings (Figure 4B). Accordingly, an asymmetric period ratio of 2:1 will yield sharp spectral features of high intensity, and thus bright and pure colors. In this respect, it should be noted that a similar bigrating period ratio (d_1:d_2) is observed in *C. opis* wings, resulting in similarly high color purity and brightness.

To investigate how structural color responds to changes in grating heights ($h_1 = h_2 = h$) between 700 and 1100 nm, bigrating transmission spectra were simulated in the visible range (between 300 and 800 nm) using different period ratios (d_1:d_2 = 1:1, 2:1, 3:1) (Figure S4, Supporting Information). When the period ratio is 1:1, spectra exhibit unsaturated colors due to the absence of sharp spectral features (Figure S4A, Supporting Information). In contrast, for period ratios of 2:1 (Figure S4B, Supporting Information) and 3:1 (Figure S4C, Supporting Information), grating structures produce far more saturated colors. However, it should be noted that the average transmittance intensity of the bigrating structure with a 3:1 period ratio is lower than the structure with a 2:1 period ratio due to increased scattering intensities at high aspect ratios.

3.3. Influence of Height Ratio (h_1:h_2) on Structural Coloration

In addition to the dependency of coloration on the period ratio, we sought to investigate how the height ratio affects structural

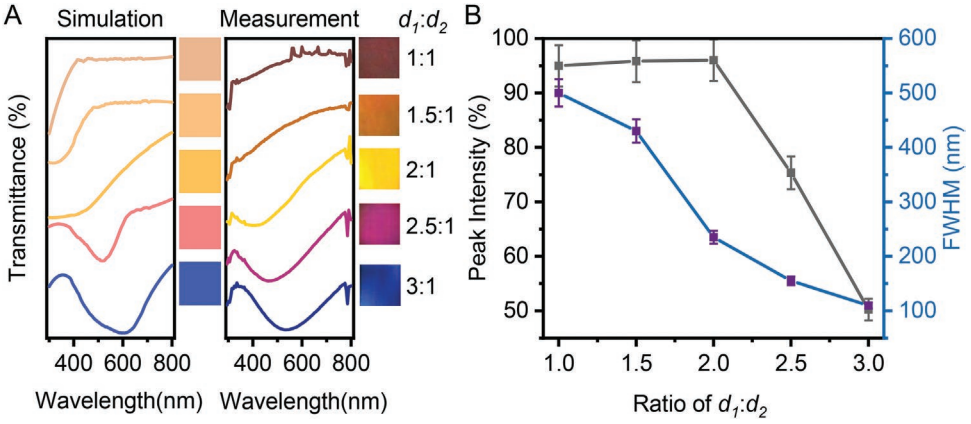

Figure 4. Influence of the period ratio (d_1:d_2) on structural coloration. A) Simulated and experimental transmission spectra and associated bigrating colors for period ratios (d_1:d_2) between 1:1 to 3:1 ($h_1 = h_2 = d_2 = 300$ nm). B) Experimentally observed peak intensity and FWHM under the same conditions. Error bars represent the standard error from 3 measurements.

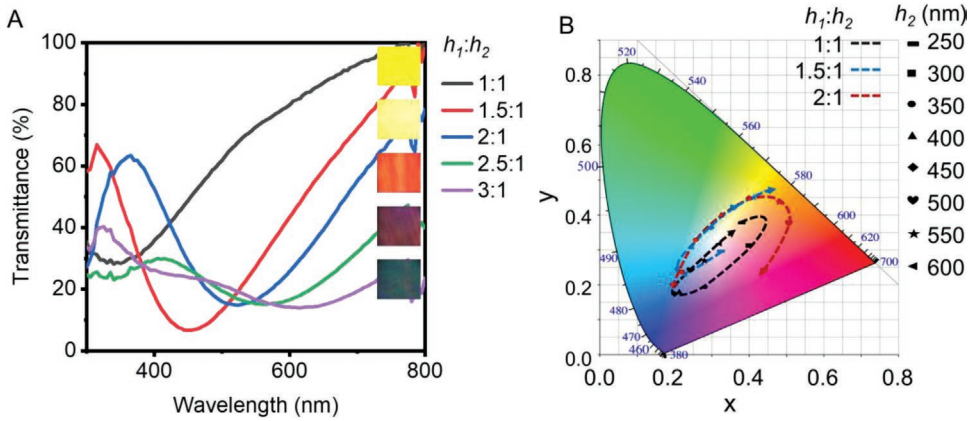

Figure 5. Influence of the height ratio (h_1:h_2) on structural coloration. A) Experimentally measured transmission spectra for bigrating structures possessing height ratios (h_1:h_2) of 1:1, 1.5:1, 2:1, 2.5:1, and 3:1, with fixed periods (d_1 = 600 nm, d_2 = 300 nm). B) Corresponding CIE 1931 chromaticity color comparison of the gratings with periods of 1.6 and 0.8 µm for height ratios of 1:1, 1.5:1, and 2:1.

coloration. Transmission spectra for bigratings with periods of 600 nm (d_1) and 300 nm (d_2) and height ratios of 1:1, 1.5:1, 2:1, 2.5:1, and 3:1 are presented in **Figure 5**A. Height ratios of 1.5:1 and 2:1 exhibit a higher transmittance when compared to larger height values (2.5:1 and 3:1), which yield unsaturated coloration and reduced transmittance. This observation can be explained by the fact that for large height ratios, significant light scattering occurs and leads to reduced transmittance.[30]

To gain further insight into color response to height ratio variations, we extracted chromaticity data (plotted in a standard CIE 1931 format and shown in Figure 5B) from the simulated transmission spectra (Figure S5, Supporting Information) for h_1:h_2 = 1:1, 1.5:1, and 2:1. As can be seen, when h_1:h_2 = 1:1, the output color shifts, in an ellipsoidal manner along the locus marked by the black dotted line. When h_1:h_2 = 1.5:1, the chromaticity coordinate sweeps over the color map from red through blue to yellow, in a semi-ellipsoidal (blue dotted line) manner similar to that observed when h_1:h_2 = 2:1. In addition, the red dotted line (h_1:h_2 = 2:1) at height values (h_2) ranging from 250 to 600 nm depicts the highest color saturation over the whole visible range compared to structures with different height ratios. Based on this analysis, it is evident that nature selects a combination of structural parameters (i.e., h_1:h_2 = 2:1) that best enhances the purity of the structural color on the wing surface.

3.4. Influence of the Period and Height Ratio on Structural Coloration

To assess the performance of the 2:1 period ratio and 2:1 height ratio bigratings in color filtration, FEM simulations were used to generate transmission spectra (**Figure 6**A,B). For a fixed height ratio (h_1:h_2 = 600 nm/300 nm) both transmittance and peak position vary moderately as a function of d_1. In contrast, transmission spectra for a fixed period ratio (d_1:d_2 = 1200 nm/600 nm) shift to longer wavelengths as h_1 is increased (Figure 6B). Specifically, a peak transmittance of 41% at 395 nm for a 500 nm/250 nm height ratio changes to 72% at 775 nm for a 1200 nm/600 nm height ratio, confirming the role of height variation in controlling inter-planar interference (Equation (1)). Comparison of Figure 6A,B indicates that variations in color are primarily controlled by height rather than the grating period. Accordingly, and based on this observation, we designed a bigrating structure for tuneable color filtering (Figure 6C). As predicted, and in agreement with the simulation data in Figure 6A,B, color variations are more sensitive to changes in height than changes in grating period. Moreover, Figure 6D presents a CIE 1931 chromaticity diagram depicting the color palettes shown in the leftmost column of Figure 6C for both simulated and measured spectra. To summarize, color variation is considerably more sensitive to changes in grating height than grating period, due to multilayer interference from both grating layers. However, in the case of thick gratings (gratings where the height is appreciably larger than the wavelength of the incident radiation), the optical pathlength difference between two layers will be large and thus no inter-planar interference will occur. Accordingly, in such a situation structural color will be more sensitive to the grating period due to the inter-rib interference of both gratings (Figure S6, Supporting Information).

To investigate the spectral characteristics in more detail, we constructed a color pallet of transmitted colors across the visible spectrum, with d_1 varying from 600 to 1100 nm (Figure S6A, Supporting Information). When the height of grating 1 (h_1) varies between 1500 and 1800 nm (with h_2 remaining constant at 1400 nm) color changes from green to yellow to red to blue. However, structures with the same period (i.e., the same values of d_1) exhibit a similar color even though h_1 varies from 1500 nm to 1800 nm. This indicates that the bigrating period plays the dominant role in adjusting hue. We then included three different color responses derived from both experimental and simulation data, for bigrating structures with d_1 = 800 nm, 1100 nm, and 1500 at a fixed height of h_1 = 1500 nm, with excellent agreement between the two approaches being evident (Figure S6B, Supporting Information). In conclusion, by tuning the height or period of the bigrating structure, we have successfully demonstrated hue- and purity-tuned structural color, which is desirable for a wide range of practical applications.

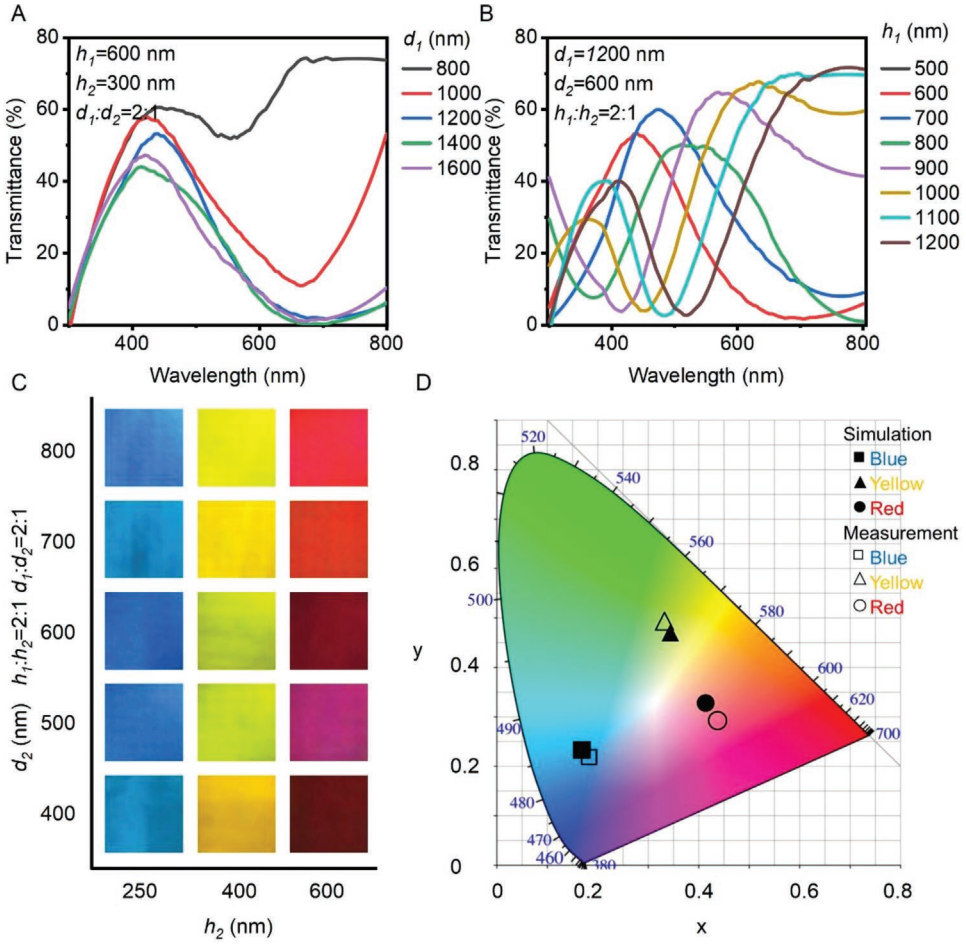

Figure 6. The influence of period and height on structural coloration. A) Simulated transmission spectra for bigrating structures with a height ratio (h_1:h_2) of 600 nm:300 nm and period (d_1:d_2) of 2:1 for different values of d_1. B) Simulated transmission spectra for bigrating structures with a period (d_1:d_2) of 1200 nm/600 nm and height ratio (h_1:h_2) of 2:1 for different values of h_1. **C**) Experimentally produced color palette of blue, yellow, and red. D) CIE 1931 chromaticity color response diagram for the leftmost column in (C), showing both simulated and experimental data.

Next, and toward the goal of achieving "full-spectrum" structural color, a structural color palette array was printed to investigate its optical properties with changes of the bigrating period. By systematically varying the grating period d_1:d_2, while keeping the grating heights (h_1 = 600 nm and h_2 = 300 nm) constant, we were able to generate a full palette of color pixels that spans the visible range, (**Figure 7**A and Figure S7, Supporting Information). Each 120 µm × 120 µm pixel presents a characteristic color that gradually changes from cyan to yellow as grating period varies. Such an approach provides a facile and direct route to the scaling-up of full-spectrum structural color patterns. Indeed, large-scale full spectrum structural color printing was further demonstrated by the high-resolution reproduction of a large painting that contains complex mixtures of the three basic colors (Figure 7B). The reproduction comprises colors of variable hue and saturation, with color transitions between neighboring color blocks appearing black due to the nature of the photo-polymerization printing process (Figure 7C). To achieve the highest possible print resolution, a 63× NA1.3 objective was used. This covers a 140 µm × 140 µm writing field of view for each block, with a pixel size of 20 µm × 20 µm. This means that the printed image is composed of 44 × 30 (W × H) blocks, corresponding to 308 × 210 pixels. Additionally, we fabricated a small segment of the original painting using a pixel size of 5 µm × 5 µm (Figure S8, Supporting Information), demonstrating the ability to both print and depict extremely fine details. These results demonstrate the utility of bigrating structures in general-purpose structural color printing and also highlight the ability to create flexible structural color devices.

4. Conclusions

As shown herein, all visible colors (with variable hue and purity) can be obtained through the design and fabrication of bigrating structures. To replicate nanoscale features of such bigrating structures, we use 2PP polymerization due to its outstanding spatial resolution and 3D structuring capability. Such bigratings are inspired by structural components found on the wings of the *C. opis* butterfly, which exhibit a striking violet-blue or blue-green coloration when the period and height of the upper grating are approximately twice as large as those of the lower grating. Through both experiments and simulations, the

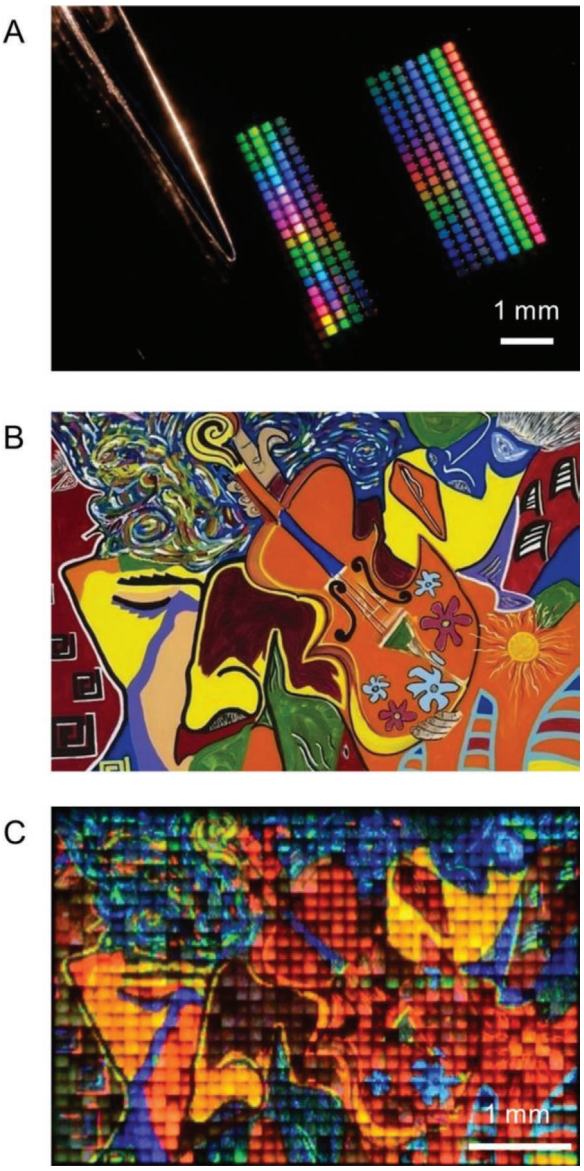

Figure 7. Image reconstruction via structural coloration. A) Image of a substrate comprising bigrating structure squares with stepwise tuning of d_1, d_2, h_1, and h_2. A sewing needle tip is placed beside the color square array to provide a sense of scale. Each square has dimensions of 120 µm × 120 µm. B) Image of a colorful painting: "Dreams of Jamaica" original painting by Ricardo Gomez (http://www.artofricardo.com/). The painting is reproduced with permission from Ricardo Gomez. C) Structural color print of the painting shown in panel (B).

dependency of structural color on the period and height of the bigratings has been assessed, with bigrating structures having a 2:1 period ratio and a 2:1 height ratio yielding enhancements in color purity due to the coupling of constructive interference and diffraction from multiple grating layers. Such an approach to structural coloration leverages structures found in living organisms and allows the generation of bespoke colors with high vibrancy and high spatial resolution. Moreover, versatile multicolor structures of this kind are likely to have numerous applications in various fields, for example, in digital 3D displays and high-density storage micro image displays. Finally, it should be noted that 2PP produces bigrating structures of consistent surface quality and optical performance; with both metrics being highly important for parallelization. However, the serial nature of the fabrication process does pose significant issues for mass production, and thus a parallel 2PP replication method is still sought after.

The results of the current study can also be used to better examine and understand the biological background of structural color. For example, the investigation of the role of structural color in the life of butterflies and natural diversity within specific populations are likely to provide considerable novel information regarding animal behavior, development, and lifespan. In the future, we aim to extend the 2PP approach to generate both ordered and disordered features within periodic nanostructures. Indeed, we believe that the introduction of disorder into the cross-rib structures will provide new and unique optical properties, such as seen in the angle-insensitivity of the blue color in *Morpho* butterfly wings[32] and the iridescent green color of the *Chrysina gloriosa* beetle.[33]

5. Experimental Section

Fabrication of the Bigrating Structures: Bigrating structures were fabricated via two-photon lithography using a Photonic Professional GT femtosecond laser lithography system (Nanoscribe GmbH, Eggenstein-Leopoldshafen, Germany) on a glass substrate coated with 10 nm indium tin oxide (ITO). Since the iridescent blue color on the wings of the *Morpho* butterfly was produced by ordered porous structures made of dielectric cuticular chitin (having a refractive index of 1.56+0.06*i*),[16] bigrating structures were manufactured from IP-Dip photoresist (Nanoscribe GmbH, Eggenstein-Leopoldshafen, Germany), which has a refractive index of 1.512.[34] During the two-photon lithography process, the laser illuminates the photoresist via a high-numerical aperture objective (63× NA 1.3) in a layer-by-layer fashion. In this way, the photoresist was solidified only in the vicinity of the laser focus, allowing the additive build-up of arbitrary 3D structures having sub-micron dimensions. A laser scanning speed of 100 mm s^{-1} and a laser power of 40 mW were used in all experiments.

Optical Measurements: Transmission spectroscopy was performed using an MSV-370 microspectrophotometer (Jasco, Tokyo, Japan) over an area of 100 × 100 μm^2. Specimens were observed using an Eclipse Ti-E inverted microscope (Nikon, Zürich, Switzerland) equipped with a Plan Apo 2× NA 0.06 objective (Nikon, Zurich, Switzerland) and a D7100 camera (Nikon, Zürich, Switzerland). Specimens were illuminated with a SPECTRA X white light LED source (Lumencor, Beaverton, USA) at a constant color temperature of 3200 K. To validate the accuracy of the structures produced by the two-photon lithography process, SEM (ULTRA 55, Zeiss, Oberkochen, Germany) and AFM (Nano-Observer, CS Instruments, Villingen-Schwenningen, Germany) measurements were also performed.

COMSOL Optical Simulations: FEM Simulations were performed using the Wave Optics Module under Perfectly Matched Layer (PML) conditions. The model was established for one unit cell of two crossed gratings using a periodic boundary condition to simulate an infinite repetition of gratings (Figure S2, Supporting Information). The grating structure was composed of a photoresist with n_r = 1.512 (IP-Dip Nanoscribe GmbH, Eggenstein-Leopoldshafen, Germany) and air. A Gaussian plane-wave at an incident angle of φ_i was used to numerically calculate variable-angle transmission spectra. The refractive index of the dielectric gratings was assumed to be dispersionless, the refractive index of the glass substrate was set to 1.47 and the absorption coefficient was considered to be negligible in the visible part of the electromagnetic spectrum. In all cases, the transverse electrical (TE) wave has the electric field component in the z direction. Transmittance was calculated from a

plane wave by integrating the near-zone scattered field (Pointing vector) over the top boundary before the PML and subsequently normalizing with respect to incident intensity.

Supporting Information

Supporting Information is available from the Wiley Online Library or from the author.

Acknowledgements

X.C. and Y.D. contributed equally to this work. The authors would like to thank Alessandro Sorrenti for assistance with AFM measurements. This work was supported by European Union's Horizon 2020 Research &Innovation Programme under the Marie Sklodowska-Curie (MSC) grant 791144, Personalized Health and Related Technologies (PHRT) (Project Nr 526), ETH Zürich, and the National Natural Science Foundation of China (Grant No.61705196).

Open access funding provided by Eidgenossische Technische Hochschule Zurich.

Conflict of Interest

The authors declare no conflict of interest.

Data Availability Statement

The data that support the findings of this study are available in the supplementary material of this article.

Keywords

3D printing, bigrating, structural colors

Received: November 12, 2021
Revised: December 10, 2021
Published online: January 23, 2022

[1] W. H. Perkin, *J. Chem. Soc. Lond.* **1862**, *14*, 230.
[2] J. Sun, B. Bhushan, J. Tong, *RSC Adv.* **2013**, *3*, 14862.
[3] K. Yu, T. Fan, S. Lou, D. Zhang, *Prog. Mater. Sci.* **2013**, *58*, 825.
[4] I. Tamáska, K. Kertész, Z. Vértesy, Z. Bálint, A. Kun, S.-H. Yen, L. P. Biró, J. Ziesmann, *J. Insect Sci.* **2013**, *13*, 87.
[5] M. Kolle, P. M. Salgard-Cunha, M. R. J. Scherer, F. M. Huang, P. Vukusic, S. Mahajan, J. J. Baumberg, U. Steiner, *Nat. Nanotechnol.* **2010**, *5*, 511.
[6] a) N. Vogel, S. Utech, G. T. England, T. Shirman, K. R. Phillips, N. Koay, I. B. Burgess, M. Kolle, D. A. Weitz, J. Aizenberg, *Proc. Natl. Acad. Sci. USA* **2015**, *112*, 10845; b) H. L. Liang, M. M. Bay, R. Vadrucci, C. H. Barty-King, J. L. Peng, J. J. Baumberg, M. F. L. De Volder, S. Vignolini, *Nat. Commun.* **2018**, *9*, 4632; c) E. S. A. Goerlitzer, R. N. K. Taylor, N. Vogel, *Adv. Mater.* **2018**, *30*, 1706654; d) L. Schertel, I. Wimmer, P. Besirske, C. M. Aegerter, G. Maret, S. Polarz, G. J. Aubry, *Phys. Rev. Mater.* **2019**, *3*, 015203; e) J. D. Forster, H. Noh, S. F. Liew, V. Saranathan, C. F. Schreck, L. Yang, J. G. Park, R. O. Prum, S. G. J. Mochrie, C. S. O'Hern, H. Cao, E. R. Dufresne, *Adv. Mater.* **2010**, *22*, 2939.
[7] a) K. X. Li, C. Li, H. Z. Li, M. Z. Li, Y. L. Song, *iScience* **2021**, *24*, 102121; b) S. Tadepalli, J. M. Slocik, M. K. Gupta, R. R. Naik, S. Singamaneni, *Chem. Rev.* **2017**, *117*, 12705.
[8] V. Saranathan, C. O. Osuji, S. G. J. Mochrie, H. Noh, S. Narayanan, A. Sandy, E. R. Dufresne, R. O. Prum, *Proc. Natl. Acad. Sci. USA* **2010**, *107*, 11676.
[9] J. P. Vigneron, P. Simonis, A. Aiello, A. Bay, D. M. Windsor, J.-F. Colomer, M. Rassart, *Phys. Rev. E* **2010**, *82*, 021903.
[10] S. Yoshioka, S. Kinoshita, *Proc. R. Soc. Lond.* **2004**, *271*, 581.
[11] A. L. Ingram, V. Lousse, A. R. Parker, J. P. Vigneron, *J. R. Soc., Interface* **2008**, *5*, 1387.
[12] W. Zhang, J. Gu, Q. Liu, H. Su, T. Fan, D. Zhang, *Phys. Chem. Chem. Phys.* **2014**, *16*, 19767.
[13] a) A. Saito, *Sci. Technol. Adv. Mater.* **2012**, *12*, 064709; b) V. Saranathan, C. O. Osuji, S. G. J. Mochrie, S. N. H. Noh, A. Sandy, E. R. Dufresne, R. O. Prum, *Proc. Natl. Acad. Sci. USA* **2010**, *107*, 11676.
[14] a) A. D. Pris, Y. Utturkar, C. Surman, W. G. Morris, A. Vert, S. Zalyubovskiy, T. Deng, H. T. Ghiradella, R. A. Potyrailo, *Nat. Photonics* **2012**, *6*, 564; b) F. Y. Zhang, Q. C. Shen, X. D. Shi, S. P. Li, W. L. Wang, Z. Luo, G. F. He, P. Zhang, P. Tao, C. Y. Song, W. Zhang, D. Zhang, T. Deng, W. Shang, *Adv. Mater.* **2015**, *27*, 1077; c) Q. S. Li, Q. Zeng, L. Shi, X. H. Zhang, K. Q. Zhang, *J. Mater. Chem. C* **2016**, *4*, 1752.
[15] Y. Ding, S. Xu, Z. L. Wang, *J. Appl. Phys.* **2009**, *106*, 074702.
[16] B. Gralak, G. Tayeb, S. Enoch, *Opt. Express* **2001**, *9*, 567.
[17] G. Zyla, A. Kovalev, E. L. Gurevich, C. Esen, Y. Liu, Y. Lu, S. Gorb, A. Ostendorf, *Appl. Phys. A* **2020**, *126*, 740.
[18] G. England, M. Kolle, P. Kim, M. Khan, P. Muñoz, E. Mazur, J. Aizenberg, *Proc. Natl. Acad. Sci. USA* **2014**, *111*, 15630.
[19] C. A. Tippets, Y. Fu, A.-M. Jackson, E. U. Donev, R. Lopez, *J. Opt.* **2016**, *18*, 065105.
[20] Y. Fu, C. A. Tippets, E. U. Donev, R. Lopez, *Wiley Interdiscip. Rev.: Nanomed. Nanobiotechnol.* **2016**, *8*, 758.
[21] B. DJ, L. ME, *Appl. Opt.* **1999**, *38*, 5282.
[22] a) P. Fiedor, J. Ortyl, *Materials* **2020**, *13*, 2951; b) B.-K. Hsiung, R. H. Siddique, D. G. Stavenga, J. C. Otto, M. C. Allen, Y. Liu, Y.-F. Lu, D. D. Deheyn, M. D. Shawkey, T. A. Blackledge, *Nat. Commun.* **2017**, *8*, 2278; c) B.-K. Hsiung, R. H. Siddique, L. Jiang, Y. Liu, Y. Lu, M. D. Shawkey, T. A. Blackledge, *Adv. Opt. Mater.* **2017**, *5*, 1600599.
[23] M. Farsari, B. N. Chichkov, *Nat. Photonics* **2009**, *3*, 450;
[24] M. F. Land, *Prog. Biophys. Mol. Biol.* **1972**, *24*, 75.
[25] a) J. P. Vigneron, P. Simonis, *Adv. Insect Physiol.* **2010**, *38*, 181; b) S. Kinoshita, S. Yoshioka, *ChemPhysChem* **2005**, *6*, 1442.
[26] J. M. Jarem, *IEEE Trans. Antennas Propag.* **1998**, *46*, 740.
[27] a) C. L. Booth, *Biol. J. Linn. Soc.* **1990**, *40*, 125; b) M. G. Meadows, M. W. Butler, N. I. Morehouse, L. A. Taylor, M. B. Toomey, K. J. McGraw, R. L. Rutowski, *J. R. Soc., Interface* **2009**, *6*, S107; c) K. Chung, S. Yu, C. Heo, J. W. Shim, S. Yang, M. G. Han, H. Lee, Y. Jin, S. Y. Lee, N. Park, J. H. Shin, *Adv. Mater.* **2012**, *24*, 2375.
[28] a) R. B. Hwang, S. T. Peng, *Appl. Opt.* **1997**, *36*, 2011; b) J. B. Harris, T. W. Preist, J. R. Sambles, R. N. Thorpe, R. A. Watts, *J. Opt. Soc. Am. A* **1996**, *13*, 2041.
[29] E. Moyroud, T. Wenzel, R. Middleton, P. J. Rudall, H. Banks, A. Reed, G. Mellers, P. Killoran, M. M. Westwood, U. Steiner, S. Vignolini, B. J. Glover, *Nature* **2017**, *550*, 469.
[30] P. Latimer, B. E. Pyle, *Biophys. J.* **1972**, *12*, 764.
[31] C. Kilchoer, U. Steiner, B. D. Wilts, *J. R. Soc., Interface* **2019**, *9*, 20180044.
[32] a) S. Kinoshita, S. Yoshioka, J. Miyazaki, *Rep. Prog. Phys.* **2008**, *71*, 076401; b) K. Watanabe, T. Hoshino, K. Kanda, Y. Haruyama, S. Matsui, *Jpn. J. Appl. Phys.* **2004**, *44*, L48.
[33] V. Sharma, M. Crne, J. O. Park, M. Srinivasarao, *Science* **2009**, *325*, 449.
[34] S. Dottermusch, D. Busko, M. Langenhorst, U. W. Paetzold, B. S. Richards, *Opt. Lett.* **2019**, *44*, 29.